Chronic overexpression of neuropeptide Y in the skin is sufficient to induce inflammation and epidermal and dermal pathology

Zoya T. Anderson
University of Alabama at Birmingham
Joseph W. Palmer
University of Alabama at Birmingham
Andrzej T. Slominski
University of Alabama at Birmingham
Jennifer L. Proctor
University of Alabama at Birmingham
Misgana I. Idris
University of Alabama at Birmingham
Dezhi Wang
University of Alabama at Birmingham
Adam E. Martin
University of Alabama at Birmingham
Melissa L. Harris (harrisml@uab.edu)
University of Alabama at Birmingham

Research Article

Keywords: Neuropeptide Y (NPY), skin physiology, pathology, McSCs, Fisher Scientific

Posted Date: October 13th, 2021

DOI: https://doi.org/10.21203/rs.3.rs-944199/v1

Abstract

Neuropeptide Y (NPY) is a pleiotropic peptide produced in the central nervous system and peripheral organs. Despite conjectures that NPY may have a role in skin physiology and pathology, the effects of NPY in this organ remain poorly understood. We reported that a knock-in mouse with entopic NPY overexpression exhibits significantly elevated NPY in the skin, accompanied by premature and progressive hair graying secondary to depletion of melanocyte stem cells within hair follicles. However, the question remains as to whether NPY overexpression in the skin can induce non-melanocyte pathology. In this study, we employed this mouse to investigate the consequences of skin-specific overexpression of NPY. Our findings show that chronic NPY overexpression in the skin induces dermal fibrosis and epidermal hyperkeratosis. Additionally, NPY overexpression induces significant accumulation of macrophages and regulatory T cells in the dermis. RNA sequencing of whole skin from NPY-overexpressing mice further reveals NPY-mediated transcriptional changes consistent with inflammatory processes and inflammation-associated skin changes and highlights novel cell types involved in the NPY-mediated response in the skin. Together, these results provide long-awaited evidence of NPY's involvement in skin pathology, providing a background for defining the precise role of NPY in the regulation of cutaneous homeostasis and disease.

Introduction:

Neuropeptide Y (NPY) is a highly conserved, 36 amino acid neuropeptide that is widely distributed throughout the nervous system and peripheral tissues [1-4]. In the central nervous system, it is mainly synthesized by sympathetic nerves or in the hypothalamus, where it plays important roles in regulation of feeding behavior and storage of energy [5-6], along with stress and anxiety responses [7-9]. Due to its wide distribution peripherally, NPY also has known roles in many biological processes, including the regulation of cell proliferation and migration [10-14], as well as immune responses [15-17].

Despite its known contributions to various physiological and pathological states, the unique roles that NPY plays in each tissue within the body are not well understood. Specifically, there is a shortage of information regarding how NPY influences skin biology. However, there has been evidence to suggest that NPY can contribute to the pathology and symptoms for an array of inflammatory skin disorders, such as psoriasis [18,19], atopic dermatitis [20-25], and vitiligo [26,27]. However, this evidence is merely correlative and there have yet to be empirical studies to elucidate the mechanism(s) by which NPY may contribute to skin pathology.

We recently identified that the B6;129S4-*Npy*^{tm2Rpa}/J mouse, which contains a knock-in mutation that induces entopic overexpression of NPY [9,28], is a novel model with which to study NPY-mediated melanocyte pathology [29]. In our previous study, we found that mice homozygous for the knock-in mutation (*Npy*$^{tet/tet}$) display premature and progressive hair graying starting at approximately 3-4 months of age in comparison to their wildtype (*Npy*$^{+/+}$) and heterozygous (*Npy*$^{tet/+}$) siblings, which do not. This hair graying is due to premature loss of melanocyte stem cells (McSCs) within the hair follicles of

Npy$^{tet/tet}$ skin. This model comes at a pivotal time in skin research because although NPY has long been implicated as a mediator of melanocyte and skin pathologies, there have yet to be any models with which to investigate these postulations. In the present study, we evaluated *Npy*$^{tet/tet}$ mice to assess whether NPY overexpression is indeed sufficient to drive non-pigmentary pathologies within the skin.

Materials And Methods:

Animals: Animal care and experimental animal procedures were approved by the Institutional Animal Care and Use Committee associated with the University of Alabama at Birmingham under the animal protocol: UAB IACUC #20382 (MLH). The procedures were performed in accordance with the guidelines set forth by this protocol. Male and female B6;129S4-*Npy*^{tm2Rpa}/J mice (RRID: IMSR_JAX:007585) were gifted from Lynn Dobrunz, PhD (UAB) and housed in standard cages separated by gender. Based on animal availability, skin from five each of 22-week-old *Npy*$^{+/+}$ and *Npy*$^{tet/tet}$ siblings was used for RNA sequencing, and a subset of these same mice (3 per genotype) was used for histopathological evaluations. Skin from three each of 35-week-old *Npy*$^{+/+}$ and *Npy*$^{tet/tet}$ siblings was used for histopathological evaluations. Hair graying was determined subjectively by macroscopic identification of the obvious and significant appearance of depigmented or gray hairs. This study is reported in accordance with ARRIVE guidelines.

Histology and Immunofluorescence

Skin harvested from the back of 22-week- and 35-week-old mice was immersed in 2% formaldehyde (Fisher Scientific, Cat# PI28908) for 30 minutes on ice. Skins were cryoprotected in 10% sucrose for at least 24 hours, embedded in Tissue Plus^{TM} O.C.T. Compound (Fisher Scientific, Cat# 23-730-571), and frozen. Due to inadequate tissue morphology achieved by cryo-sectioning, reserved skins that were frozen in blocks were alternatively prepared for paraffin sectioning. Frozen skins were thawed in 4% formaldehyde for 1 hour and transferred to fresh 4% formaldehyde for further fixation overnight. These skins were embedded in paraffin at the Pathology Core Research Lab (UAB) followed by sectioning with a microtome at 5µm thickness. Hematoxylin and eosin, as well as Toluidine blue, staining was performed on skin sections at the Pathology Core Research Lab (UAB).

For immunolabeling, sections were immersed in CitriSolv (Fisher Scientific, Cat# 22-143-975) for 5 minutes twice, followed by two 5-minute immersions in 100% ethanol. These slides underwent one 3-minute immersion in 75% ethanol, followed by one 3-minute immersion in 50% ethanol. Slides were washed twice for 5 minutes in DPBS (Fisher Scientific, Cat# 14-190-250) with 0.1% Tween 20 (Fisher Scientific, Cat# BP337500). Sections were incubated with primary antibody overnight at 4°C. Primary antibodies that were used include those against F4/80 (1:100, rat anti-mouse, Thermo Fisher Scientific, Cat# 14-4801-82, RRID: AB_467558), CD3 (1:100, rat anti-mouse, Thermo Fisher Scientific, Cat# 14-0032-82, RRID: AB_467053), FOXP3 (1:100, rat anti-mouse, Thermo Fisher Scientific, Cat# 14-5773-82, RRID: AB_467576). After washing, sections were incubated with the appropriate secondary antibodies (1:1000; AlexaFluor, Invitrogen) for 1 hour at room temperature. Sections were washed and mounted with

Prolong™ Gold Antifade Mountant with DAPI (Thermo Fisher Scientific, Cat# P36931). Prior to incubation with primary antibody against F4/80, sections underwent antigen retrieval with 10µg/mL of Proteinase K (Fisher Scientific, Cat# BP1700-100) at 37ºC for 10 minutes, followed by a 5-minute wash in DPBS with 0.1% Tween 20. Macrophages and T cells were defined as cells that were positive for both DAPI and antigen. Quantitation of antigen+ cells was performed by taking images along the length of skin sections and counting the number of positive cells within the skin. All analyses were performed blind to the genotype. Fluorescence and bright-field microscopy were performed on a Nikon Eclipse 80i microscope, captured using Nikon NIS Elements software (NIS-Elements, RRID:SCR_014329), and images were processed using Adobe Photoshop (RRID: SCR_014199).

RNA isolation and quantitative PCR

Skin for quantitative PCR (qPCR) and RNAseq analysis was harvested in TRIzol reagent (Thermo Fisher Scientific, Cat# 15-596-018) and homogenized using a bead homogenizer (MP Biomedicals). Total RNA from skin was purified using the RNAEasy MiniKit (Qiagen) after phenol/chloroform separation.

For qPCR analysis, 1-1.5 µg of RNA was reverse transcribed using the High Capacity cDNA Reverse Transcription Kit (Thermo Fisher Scientific, Cat# 4364103). qPCR was performed using the following TaqMan gene expression assays: *Npy* (Mm03048253_m1, Thermo Fisher Scientific, Cat# 4331182) and the Mouse GAPD Endogenous Control (Thermo Fisher Scientific, Cat# 4352339E). A standard curve was used to determine relative quantity based on C_t values. Relative expression of the target gene was determined by dividing its relative quantity by the endogenous control gene relative quantity.

RNA sequencing

Sequencing of mRNA was performed on the Illumina NextSeq500 as described by the manufacturer (Illumina Inc., San Diego, CA). Briefly, RNA quality was assessed using the Agilent 2100 Bioanalyzer. RNA with a RNA Integrity Number (RIN) of ≥7.0 was used for sequencing library preparation. RNA passing quality control was converted to a sequencing ready library using the NEBNext Ultra II Directional RNA library kit as per the manufacturer's instructions (polyA mRNA workflow; NEB, Ipswich, MA). The cDNA libraries were quantitated using qPCR in a Roche LightCycler 480 with the Kapa Biosystems kit for Illumina library quantitation (Kapa Biosystems, Woburn, MA) prior to cluster generation. Cluster generation was performed according to the manufacturer's recommendations for onboard clustering (Illumina, San Diego, CA). We generated between 30-35 million paired end 75bp sequencing reads per sample for transcript level abundance.

Read quality of fastq files was assessed using FastQC (v0.11.8; RRID:SCR_014583) and trimming was performed using Trimmomatic (v0.36; RRID:SCR_011848). Reads were aligned to the Ensembl (RRID:SCR_002344) mouse mm10 reference genome with the STAR (v2.5.2; RRID:SCR_015899) aligner software using default parameters and count tables were generated using the STAR genecounts feature and full Ensembl GTF annotation file. Differential gene expression analysis performed using DESeq2

(v1.30.1; RRID:SCR_015687) package in R using default settings. All sequencing data generated in this study is available at NCBI GEO under accession GSE183831.

Heatmaps were generated by applying the regularized log transformation (rlog) to the results data frame produced by the DESeq2 package. To generate figures, values for filtered genes of interest were loaded into the pheatmap (v1.0.12; RRID:SCR_016418) R package and scaled by row.

Clustered bar graphs were generated by using Gene Ontology Biological Process, Cell Type signature gene sets, and Human Phenotype Ontology analyses performed using the molecular signatures database (MSigDB v6.2, RRID:SCR_016863) through the Gene Set Enrichment Analysis website platform. Visualization of data was performed using the ggplot2 (v3.3.3; RRID:SCR_014601) R-package. PCA plots were also generated using ggplot2 on the rlog file generated by DESeq2.

Statistical analysis: All data are presented as mean ± standard deviation and were analyzed using GraphPad Prism 9 (RRID: SCR_002798) statistical software. Unpaired t-tests were applied for statistical comparison of histological measurements and immune cell count data. p-values of < 0.05 were considered a statistically significant difference.

Results:

1. $Npy^{tet/tet}$ skin is fibrotic with hyperkeratosis

To interrogate whether skin pathologies are present in *$Npy^{tet/tet}$* mice, we performed histopathological evaluations on the dorsal skin of 22-week-old (i.e., pre-graying stage; [9]) and 35-week-old (i.e., post-graying stage; [9]) *$Npy^{+/+}$* and *$Npy^{tet/tet}$* mice (Figure 1). 22-week-old *$Npy^{tet/tet}$* skin appears to exhibit epidermal thickening with hyperkeratosis, compared to their *$Npy^{+/+}$* littermates, as evidenced by hematoxylin and eosin (H&E) stained sections (Figure 1A). Following this observation, we quantified the thickness of each layer of the skin (epidermis, dermis, and subcutaneous adipose tissue). Between *$Npy^{+/+}$* and *$Npy^{tet/tet}$* mice, no difference was found in the thickness of the whole skin, dermis, or subcutaneous adipose tissue, however, the epidermis of 22-week-old *$Npy^{tet/tet}$* skin is significantly thicker than that of *$Npy^{+/+}$* skin (Figure 1B). At 35 weeks old, hyperkeratosis (Figure 1C, D) in *$Npy^{tet/tet}$* skin persists, and fibrosis, evidenced by an increased abundance of pink collagen fibers, is now observed in the dermis. No differences between the genotypes are observed in the thickness of the dermis or subcutaneous adipose tissue at this timepoint. These findings indicate that chronic overexpression of NPY in the skin is sufficient to induce functional changes in epidermal keratinocytes and dermal fibroblasts that is pathological.

2. $Npy^{tet/tet}$ skin is infiltrated by macrophages and T cells

Following the identification of dermal fibrosis and epidermal thickening in *$Npy^{tet/tet}$* skin, we questioned what mechanisms would contribute to these NPY-induced pathologies. Knowing that NPY has diverse

functions on immune cells, including pro-inflammatory and anti-inflammatory effects [13, reviewed in (17), 30], we hypothesized that NPY can induce macrophage infiltration and can increase T cell proliferation in the skin [14, 31-34]. Accordingly, we assessed immunolabeled macrophages (F4/80) and T cells (CD3) to determine the average number of these immune cells within the skin of 22- and 35-week-old mice (Figures 2 and 3). Macrophages are significantly more abundant in the skin of 22-week-old *Npy*$^{tet/tet}$ mice when compared to their *Npy*$^{+/+}$ littermates (Figure 2A,B). This accumulation of macrophages is observed in the dermis and subcutaneous adipose tissue of *Npy*$^{tet/tet}$ skin. At 35 weeks of age, chronic NPY overexpression induces an increase in macrophages in the dermis of *Npy*$^{tet/tet}$ skin, but this increase was only statistically significant at a less stringent p-value of 0.1 (Figure 2C,D).

We previously reported no overt qualitative changes in the abundance of CD4$^+$ and CD8$^+$ T cells in *Npy*$^{tet/tet}$ skin [29], yet using the pan T cell marker and quantitative assessment we find that T cells are significantly more abundant in *Npy*$^{tet/tet}$ skin compared to *Npy*$^{+/+}$ littermates at 22 and 32 weeks old. This is attributable to T cell accumulation in the dermis and a trend for their accumulation in the adipose tissue (Figure 3A,B). This pattern persists in 35-week-old *Npy*$^{tet/tet}$ skin (Figure 3C,D). To further characterize the T cell pool, we assessed for the abundance of regulatory T cells (Tregs) via FOXP3 expression. In 22-week-old skin, Tregs are significantly more abundant in *Npy*$^{tet/tet}$ skin, which is attributed to their significant accumulation in the dermis (Figure 4A,B). This persists in 35-week-old skin, along with a trend for their accumulation in the adipose tissue (Figure 4C,D). Tregs are known to express FOXP3 as well as CD4 [35]. Although we previously observed no qualitative differences in CD4$^+$ T cell abundance [29], the improved quality of the paraffin-embedded tissues used in the current study compared to the frozen tissue used in our previous study revealed quantitative differences in T cells expressing the FOXP3 marker for Tregs. These findings suggest that chronic NPY overexpression in the skin can induce infiltration or proliferation of macrophages and T cells, specifically Tregs, resulting in a chronically inflamed environment within the skin.

NPY has also been shown to induce mast cell activation [36]. Accordingly, we assessed for NPY-mediated changes in mast cell numbers within 22-week-old *Npy*$^{+/+}$ and *Npy*$^{tet/tet}$ skin and found that mast cells are similarly abundant in the skin of both genotypes (**Supplementary Figure 5**). Pathological phenotypes, by H&E staining and immunolabeling, are also observed in heterozygous *Npy*$^{tet/+}$ mice and these phenotypes are generally similar to *Npy*$^{tet/tet}$ mice or are intermediate between those observed in *Npy*$^{+/+}$ and *Npy*$^{tet/tet}$ mice (**Supplementary Figures 1-4**).

3. Transcriptional changes in 22-week-old Npy$^{tet/tet}$ skin further supports inflammation as a major response to chronic NPY overexpression and a contributing factor to NPY-mediated skin pathologies

To identify transcriptional changes in the skin that might elaborate the mechanisms by which NPY induces skin pathology and inflammation, we harvested whole skin from 22-week-old *Npy*$^{+/+}$ and *Npy*$^{tet/tet}$ mice to be assessed by RNA sequencing (RNAseq) (Figure 5A). *Npy* upregulation observed by RNAseq was independently validated in skin from a different anatomical region of the same mice via

qPCR (Figure 5B). From this RNAseq data we made several comparisons; all *Npy*$^{tet/tet}$ versus all *Npy*$^{+/+}$ samples, *Npy*$^{tet/tet}$ versus *Npy*$^{+/+}$ samples based on sex, an intra-genotype evaluation of *Npy*$^{tet/tet}$ samples (Figure 5C). When comparing *Npy*$^{tet/tet}$ animals to *Npy*$^{+/+}$ littermates, a short list of 32 differentially expressed genes (DEGs; $-1 > \log_2 FC < 1$, padj < 0.05) was obtained. Six of these DEGs were upregulated. When comparing gene signatures specific to a certain cell type and biological process were most apparent in the downregulated genes. Twenty-six of 32 DEGs were downregulated— 11 of these DEGs were related to melanogenesis and pigmentation, such as *Dct*, *Mc1r*, *Pmel*, and *Tyr*, and 4 of these DEGs are usually expressed in anagen-stage mouse hair follicle keratinocytes, including *Dlx2*, *Dlx3*, *Msx2*, *Mycn* (Figure 5D) [37,38].

By principal component analysis (PCA), we noticed that our RNAseq samples clustered somewhat by sex rather than by genotype (Supplementary Figure 6). Thus, repeating the differential expression analysis while only comparing *Npy*$^{tet/tet}$ to *Npy*$^{+/+}$ animals of the same sex revealed some of the same DEGs as above along with additional DEGs not apparent when the samples of both sexes were evaluated together (see overlaps in Figure 5D). Interestingly, comparing male mice only (*Npy*$^{tet/tet}$ males (n=2) versus *Npy*$^{+/+}$ males (n=3)) showed an upregulation of *Retnla*, a gene which participates in the negative regulation of Th2 responses and induction of fibrosis and is upregulated in response to IL-4 and IL-13 in macrophages [39-41]. *Npy*$^{tet/tet}$ males also downregulated *Skint3* and *Skint9*. These genes are expressed by epidermal keratinocytes to signal dendritic epithelial T cells to promote proper skin wound healing and are downregulated during skin aging [42]. On the other hand, comparing *Npy*$^{tet/tet}$ and *Npy*$^{+/+}$ females only [*Npy*$^{tet/tet}$ females (n=3) versus *Npy*$^{+/+}$ females (n=2)], we discovered an abundance of new DEGs only significant in this sex (67 total). This included 9 upregulated genes, 4 of which are involved in adipogenesis and lipogenesis, *Sult1e1, Thrsp, Fasn, Agpat2* [43-45], and one *Pla2g2d*, that is known as a pro-resolving lipid mediator that works to terminate inflammation [46]. The remainder of the DEGs downregulated by *Npy*$^{tet/tet}$ females are enriched in genes expressed by various layers of anagen-stage hair follicles, including *Cryba4, Edn2, Fbp1, Fgf5, Foxe1, Krt28, Krt31, Krt33a, Krt35, Krt71, Krtap11-1, Krtap15, Padi3, S100a3, Sct, Scl39a8*, and *Tchh*. It is unclear, however, whether this downregulation of hair follicle-related genes is reflective of an NPY-related pathology or differences in the hair stage of *Npy*$^{tet/tet}$ and *Npy*$^{+/+}$ females at harvest as only a subset of these animals was evaluated for histopathology.

Previously we reported that the onset of macroscopic hair graying in the *Npy*$^{tet/tet}$ mice initiates at 25-27 weeks [29], yet this timeframe is variable as graying was visible in a subset of this cohort of mice as early as 22 weeks (Figure 5A). Interested in interrogating transcriptomic signatures that might explain the accelerated onset of graying in the “gray” subset of *Npy*$^{tet/tet}$ mice, we reanalyzed our RNAseq data from the 22-week-old skin to compare the “gray” and “non-gray” *Npy*$^{tet/tet}$ mice. Interestingly, the gray subset is comprised of male *Npy*$^{tet/tet}$ mice, while the non-gray subset contains female *Npy*$^{tet/tet}$ mice. By PCA analysis, *Npy*$^{tet/tet}$ animals clustered independently based on both graying and sex with 71% variance across principal component 1 (PC1) (Figure 6A). *Npy*$^{+/+}$ animals also cluster independently across PC1 based on sex, yet with only 57% variance. This suggests that the additional variance seen between

Npy$^{tet/tet}$ animals across PC1 may be explained by DEGs that are specific to graying. It is important to note that although the male *Npy*$^{tet/tet}$ mice of this particular 22-week-old cohort exhibited hair graying before their female counterparts, this male-first presentation of the phenotype is not consistent across multiple litters (data not shown).

To identify the genes that contribute to graying onset within the gray cohort of *Npy*$^{tet/tet}$ mice, we first removed any DEGs that could be considered sex-associated and may be confounding. First, differential expression analysis between the sexes was performed for each genotype and a list containing both upregulated and downregulated genes for each contrast were generated (*Npy*$^{tet/tet}$ males versus *Npy*$^{tet/tet}$ females = 918 DEGS; and *Npy*$^{+/+}$ males versus *Npy*$^{+/+}$ females = 303 DEGs). Next, we overlapped these two DEG lists and removed the 138 genes which were present in both lists and which we deemed to be common, sex-associated genes (Figure 6B). The remaining 780 DEGs within the *Npy*$^{tet/tet}$ group were evaluated via gene set enrichment analysis (GSEA) to investigate the transcriptomic differences between gray (i.e., male) and non-gray (i.e., female) *Npy*$^{tet/tet}$ skin.

GSEA to identify the biological processes upregulated in non-gray *Npy*$^{tet/tet}$ skin indicates that immune system development is the second-most enriched process. Specifically, the processes of lymphocyte activation, interleukin-4 (IL-4) production, and cell proliferation are among the most enriched and match expectations based on known NPY signaling. Additionally, processes such as thermogenesis and neurogenesis are enriched in non-gray *Npy*$^{tet/tet}$ skin (**Supplementary File**). Conversely, GSEA shows that epidermal cell differentiation is the third-most enriched process in gray *Npy*$^{tet/tet}$ skin. Additionally, myeloid leukocyte (i.e., macrophage) activation and response to cytokines are enriched in the skin of gray *Npy*$^{tet/tet}$ mice (Figure 6C). Despite the gray *Npy*$^{tet/tet}$ mice clearly exhibiting a more progressed graying phenotype, the expression of pigment genes is not consistently up- or down-regulated in either subset of the *Npy*$^{tet/tet}$ group. Interestingly, genes related to T cells and B cells are more enriched in the non-gray *Npy*$^{tet/tet}$ skin, while genes related to macrophages are enriched in the gray *Npy*$^{tet/tet}$ skin (Figure 6D). This observation is further supported by GSEA for the cell types that are enriched in the skin of each subset of the *Npy*$^{tet/tet}$ genotype. The transcriptome of non-gray *Npy*$^{tet/tet}$ skin shows high enrichment for cells of neural origin (**Supplementary File**), as well as enrichment for fibroblasts and immune cells, more specifically B cells (Figure 6E). This contrasts with gray *Npy*$^{tet/tet}$ skin, in which dendritic cells, proliferating macrophages, and proliferating basal cells are within the 10 most enriched cell types (Figure 6E). These changes in transcriptomic signatures from non-gray to gray may reflect a progression in cellular pathology that ultimately drives the more severe hypopigmentation observed in 35-week-old mice.

GSEA to identify human phenotypes with similar gene enrichment profiles indicates that abnormal function in the human gastrointestinal tract and personality abnormalities, including depressivity, are among the only 5 human phenotypes with similar gene enrichment as the non-gray *Npy*$^{tet/tet}$ skin, the former of which could be due to the upregulation of immune cell activation in non-gray skin (Figure 6F). The same GSEA shows that gray *Npy*$^{tet/tet}$ skin gene enrichment is similar to that of multiple hair

abnormalities, with alopecia being the most similar human phenotype (**Supplementary File**). Notably, gray *Npy*$^{tet/tet}$ skin is highly enriched for abnormal hair growth, thickened skin, and hyperkeratosis (Figure 6F), which match our histopathological findings (Figure 1).

Discussion:

Skin neuroendocrinology literature has long suggested the involvement of NPY in skin pathology [47]. In support of this hypothesis, clinical studies have shown that genetic mutations in *NPY* are associated with increased susceptibility for vitiligo [48-49]. Studies have also shown that NPY is more highly expressed in the circulation and affected skin from patients suffering from atopic dermatitis and vitiligo [20-25,27]. Despite these long-standing theories and correlative data from the clinic, there has yet to be definitive data to show whether and how NPY is involved in skin pathology.

We previously reported that chronic, entopic overexpression of NPY induces McSC depletion from murine hair follicles to result in premature and progressive hair graying [29]. This McSC loss and hair graying are associated with elevated expression of *Npy* in the skin, with NPY protein being elevated in multiple skin cell types. Our previous results were reminiscent of what has been found in some vitiligo patients, where NPY is elevated in the depigmented skin [27], leading us to further inquire into whether this skin-specific elevation of NPY in the *Npy*$^{tet/tet}$ mouse may also be relevant to other skin pathologies.

In the present study, we show that chronic overexpression of NPY in *Npy*$^{tet/tet}$ skin induces epidermal hyperkeratosis by 22 weeks of age, which persists, along with the presentation of dermal fibrosis, at 35 weeks of age (Figure 1). Epidermal thickening in *Npy*$^{tet/tet}$ skin is in line with similar histopathology that is seen in mouse models of atopic dermatitis [50]. Additionally, we show that inflammation plays a role in these skin pathologies, indicated by increased macrophage infiltration and increased Treg abundance in the dermis at 22 weeks old, the latter of which persisted at 35 weeks (Figures 2 and 3). Likewise, increased abundance of macrophages and T cells have been shown in the skin of mouse models of atopic dermatitis [50]. RNAseq data from whole skin of 22-week-old *Npy*$^{+/+}$ and *Npy*$^{tet/tet}$ mice reveal that genes involved in pigmentation, proper wound healing, and the hair follicle are downregulated in response to chronic NPY overexpression (Figure 5), while genes that promote fibrosis, adipocyte functions, and inflammatory responses are upregulated. Our RNAseq findings also suggest mechanisms that may contribute to the differential progression of hair graying in response to NPY in the skin. In 22-week-old *Npy*$^{tet/tet}$ skin with advanced presentation of hair graying, *Npy* is more highly expressed, and there is gene enrichment for macrophage activation and keratinocyte differentiation. In contrast, non-gray *Npy*$^{tet/tet}$ skin has lower *Npy* expression and is enriched for lymphocyte activation and cell proliferation (Figure 6). These differences in the enrichment for different immune cell populations, biological processes, and cell types in gray versus non-gray *Npy*$^{tet/tet}$ skin suggest that the level of *Npy* expression may influence the progression of skin inflammation and pathology. Additionally, these differences could explain the wide variances in the pathological characteristics that we have shown within the skin of *Npy*$^{tet/tet}$ mice (Figures 1-4). As a note, the accelerated graying observed in this cohort of mice was also associated with

the male gender, but this male-first presentation was not consistent across *Npy*$^{tet/tet}$ mice in other litters. While NPY has been linked to sex-specific biological changes, we hesitate to make similar conclusions here without further evaluation.

Using the Crowd function from the online Enrichr database, we further compared our gene datasets to previously published datasets [51-53]. Interestingly, DEGs identified from the skins of both gray and non-gray *Npy*$^{tet/tet}$ mice are similar to that of human and mouse samples of psoriasis and atopic dermatitis. These similarities are largely due to increased expression of *Gjb2*, *Krt27*, *Krt33a*, *Psors1c2*, and *Fabp5* in gray *Npy*$^{tet/tet}$ skin, which have been shown to be significantly upregulated in skin from mouse models of psoriasis and in human psoriatic skin [54-56]. Likewise, transcripts for *Ecm2* and *Plscr4* are reduced in non-gray *Npy*$^{tet/tet}$ skin, and the downregulation of these genes has been associated with human atopic dermatitis and psoriasis, respectively [55,57]. The dysregulation of a number of genes in *Npy*$^{tet/tet}$ skin that are similarly dysregulated in samples of psoriasis and atopic dermatitis suggests that overexpression of NPY may influence the skin's transcriptional landscape that mirrors aspects of these diseases.

Altogether, our findings provide the long-awaited evidence that NPY can indeed have a pathomechanistic role in the skin. In *Npy*$^{tet/tet}$ skin, NPY overexpression is sufficient to induce epidermal thickening, hyperkeratosis, dermal fibrosis, and macrophage and Treg accumulation in the dermis. These histopathologies are reminiscent of pathological hallmarks that are seen in human and mouse skin affected by atopic dermatitis or psoriasis. For example, skin affected by atopic dermatitis has been shown to have a T-helper 2 (Th2) immune profile that is accompanied by increased numbers of Tregs [58,59], both of which are present in our findings from RNAseq and histological evaluations, respectively. Furthermore, it has been shown that psoriatic skin exhibits epidermal thickening and macrophage infiltration (reviewed in [60]), two pathological findings identified in our study.

Gene enrichment within *Npy*$^{tet/tet}$ skin supports the pathological findings of NPY-induced inflammation and epidermal thickening, along with reduction in pigment genes. The current study, along with the findings from our previous study, suggests that the B6;129S4-*Npy*^{tm2Rpa}/J mouse line is a novel model that can be used to further evaluate NPY-mediated inflammatory skin pathologies. For instance, RNAseq analysis indicated that gene signatures for B cells and NK cells are enriched in non-gray *Npy*$^{tet/tet}$ skin, and signatures for dendritic cells are enriched in gray *Npy*$^{tet/tet}$ skin. Thus, future studies to evaluate the prevalence of these immune cells in the skin of *Npy*$^{tet/tet}$ mice will determine whether these cells are also involved in the skin inflammation that is induced by NPY overexpression.

Although vitiligo is the inflammatory skin disease whose primary phenotype is a loss of skin color, or hypopigmentation, other inflammatory skin diseases have also been shown to induce hypopigmentation. There have been severe cases of psoriasis and atopic dermatitis that have been reported to induce skin hypopigmentation in a process termed post-inflammatory hypopigmentation [61-63]. By mechanisms that remain unclear, post-inflammatory hypopigmentation occurs when chronic cutaneous inflammation

induces epidermal melanocyte dysfunction or loss, resulting in temporary or permanent loss of skin color, respectively (reviewed in [64]). Our findings that inflammation in *Npy*$^{tet/tet}$ skin precedes hair graying, and that inflammation persists following hair graying, suggests that overexpression of NPY in the skin may be a contributory mechanism to post-inflammatory hypopigmentation. Future studies with this knock-in mouse line should investigate the order by which inflammation and other skin tissue changes (e.g., hyperkeratosis) occur in *Npy*$^{tet/tet}$ skin. This will elucidate the primary pathological effect of NPY in the skin and identify a potential pathway that can be targeted to mitigate early detrimental effects of NPY. Additional mechanistic studies to investigate specific cellular responses to NPY overexpression (e.g., using in vitro approaches and/or conditional knock-out of Y receptors in specific cell types) will be important to identify the critical cell mediators of the NPY response in the skin. Finally, the *Npy*$^{tet/tet}$ mouse now allows for novel evaluations into NPY's contribution to skin pathology in the context of other models of skin disease.

Declarations

Acknowledgements

This research was supported by start-up funding provided to MLH by the Department of Biology and the College of Arts and Sciences at the University of Alabama at Birmingham. This research was also supported by the grant ID# 67038665 from Pfizer to MLH. ATS was supported by 1R01AR073004-01A1, R01AR071189-01A1, VA merit grant (no. 1I01BX004293-01A1), and R21 AI149267-01A1. Fellowship support was also provided independently to ZTA (UAB Blazer Fellow, NSF LSAMP Fellow).

Conflicts of Interest

All authors declare no conflicts of interest.

Author Contributions

DW and AEM performed paraffin embedment and sectioning of tissues, as well as H&E and Toluidine Blue staining. ATS performed histopathological evaluations for H&E-stained tissue. JLP and ZTA performed quantitation of tissue thickness. ZTA performed immunofluorescent cell labeling and performed all cell number quantifications. ZTA and MLH analyzed and interpreted data. JWP performed bioinformatic analysis of the RNAseq data. JWP, MLH, and ZTA generated figures to represent RNAseq findings. ZTA and MII performed qPCR experiments. ZTA, ATS, and MLH drafted the manuscript. All authors reviewed the manuscript and approved its submission.

Availability of data and materials

The datasets supporting the findings of this study are available in NCBI GEO under accession GSE183831.

References

1. Dumont, Y., Martel, J., Fournier, A., Stpierre, S. & Quirion, R. Neuropeptide Y and neuropeptide Y receptor subtypes in brain and peripheral tissues. *Progress in Neurobiology* **38**, 125–167 (1992).
2. Palmiter, R. D., Erickson, J. C., Hollopeter, G., Baraban, S. C. & Schwartz, M. W. Life without neuropeptide Y. *Recent Prog. Horm. Res.* **53**, 163–199 (1998).
3. Cerdá-Reverter, J. M. & Larhammar, D. Neuropeptide Y family of peptides: structure, anatomical expression, function, and molecular evolution. *Biochem. Cell Biol.* **78**, 371–392 (2000).
4. Silva, A. P., Cavadas, C. & Grouzmann, E. Neuropeptide Y and its receptors as potential therapeutic drug targets. *Clin Chim Acta* **326**, 3–25 (2002).
5. Kalra, S. P., Dube, M. G., Sahu, A., Phelps, C. P. & Kalra, P. S. Neuropeptide Y secretion increases in the paraventricular nucleus in association with increased appetite for food. *Proc. Natl. Acad. Sci. U.S.A.* **88**, 10931–10935 (1991).
6. Balasubramaniam, A., Sheriff, S., Zhai, W. & Chance, W. T. Bis(31/31'){[Cys31, Nva34]NPY(27–36)-NH2}: a neuropeptide Y (NPY) Y5 receptor selective agonist with a latent stimulatory effect on food intake in rats. *Peptides* **23**, 1485–1490 (2002).
7. Kokare, D. M., Dandekar, M. P., Chopde, C. T. & Subhedar, N. Interaction between neuropeptide Y and alpha-melanocyte stimulating hormone in amygdala regulates anxiety in rats. *Brain Res.* **1043**, 107–114 (2005).
8. Hirsch, D. & Zukowska, Z. NPY and Stress 30 Years Later: The Peripheral View. *Cell Mol Neurobiol* **32**, 645–659 (2012).
9. Corder, K. M. *et al.* Overexpression of neuropeptide Y decreases responsiveness to neuropeptide Y. *Neuropeptides* **79**, 101979 (2020).
10. Shigeri, Y. & Fujimoto, M. Neuropeptide Y stimulates DNA synthesis in vascular smooth muscle cells. *Neurosci Lett* **149**, 19–22 (1993).
11. Movafagh, S. *et al.* Neuropeptide Y induces migration, proliferation, and tube formation of endothelial cells bimodally via Y1, Y2, and Y5 receptors. *FASEB j.* **20**, 1924–1926 (2006).
12. Kuo, L. E. *et al.* Neuropeptide Y acts directly in the periphery on fat tissue and mediates stress-induced obesity and metabolic syndrome. *Nat Med* **13**, 803–811 (2007).
13. Singer, K. *et al.* Neuropeptide Y Is Produced by Adipose Tissue Macrophages and Regulates Obesity-Induced Inflammation. *PLoS ONE* **8**, e57929 (2013).
14. Choi, B. *et al.* Elevated Neuropeptide Y in Endothelial Dysfunction Promotes Macrophage Infiltration and Smooth Muscle Foam Cell Formation. *Front. Immunol.* **10**, 1701 (2019).
15. Wheway, J. *et al.* A fundamental bimodal role for neuropeptide Y1 receptor in the immune system. *J. Exp. Med.* **202**, 1527–1538 (2005).
16. Dimitrijević, M. & Stanojević, S. The intriguing mission of neuropeptide Y in the immune system. *Amino Acids* **45**, 41–53 (2013).

17. Chen, W. *et al.* Neuropeptide Y Is an Immunomodulatory Factor: Direct and Indirect. *Front. Immunol.* **11**, 580378 (2020).
18. Reich, A. & Szepietowski, J. C. Vasoactive peptides in the pathogenesis of psoriasis. *G Ital Dermatol Venereol* **143**, 289–298 (2008).
19. Gao, T. *et al.* The Neuropeptide Y System Regulates Both Mechanical and Histaminergic Itch. *J Invest Dermatol* **138**, 2405–2411 (2018).
20. Pincelli, C., Fantini, F., Massimi, P. & Giannetti, A. Neuropeptide Y-like immunoreactivity in Langerhans cells from patients with atopic dermatitis. *Int J Neurosci* **51**, 219–220 (1990a).
21. Pincelli, C. *et al.* Neuropeptides in skin from patients with atopic dermatitis: an immunohistochemical study. *Br. J. Dermatol.* **122**, 745–750 (1990b).
22. Tobin, D. *et al.* Increased number of immunoreactive nerve fibers in atopic dermatitis. *J Allergy Clin Immunol* **90**, 613–622 (1992).
23. Salomon, J. & Baran, E. The role of selected neuropeptides in pathogenesis of atopic dermatitis. *J Eur Acad Dermatol Venereol* **22**, 223–228 (2008).
24. Oh, S. H. *et al.* Association of stress with symptoms of atopic dermatitis. *Acta Derm Venereol* **90**, 582–588 (2010).
25. Hodeib, A. *et al.* Nerve growth factor, neuropeptides and cutaneous nerves in atopic dermatitis. *Indian J Dermatol* **55**, 135–139 (2010).
26. Lazarova, R., Hristakieva, E., Lazarov, N. & Shani, J. Vitiligo-related neuropeptides in nerve fibers of the skin. *Arch. Physiol. Biochem.* **108**, 262–267 (2000).
27. Tu, C., Zhao, D. & Lin, X. Levels of neuropeptide-Y in the plasma and skin tissue fluids of patients with vitiligo. *J. Dermatol. Sci.* **27**, 178–182 (2001).
28. Marie, L. Ste., Luquet, S., Cole, T. B. & Palmiter, R. D. Modulation of neuropeptide Y expression in adult mice does not affect feeding. *Proceedings of the National Academy of Sciences* **102**, 18632–18637 (2005).
29. Anderson, Z. T., Mehl, J., Corder, K. M., Dobrunz, L. E. & Harris, M. L. A novel mouse model to evaluate neuropeptide Y-mediated melanocyte pathology. *Experimental Dermatology* exd.14406 (2021) doi:10.1111/exd.14406.
30. Oda, N. *et al.* Requirement for neuropeptide Y in the development of type 2 responses and allergen-induced airway hyperresponsiveness and inflammation. *American Journal of Physiology-Lung Cellular and Molecular Physiology* **316**, L407–L417 (2019).
31. De la Fuente, M., Bernaez, I., Del Rio, M. & Hernanz, A. Stimulation of murine peritoneal macrophage functions by neuropeptide Y and peptide YY. Involvement of protein kinase C. *Immunology* **80**, 259–265 (1993).
32. Straub, R. H. *et al.* Neuropeptide Y cotransmission with norepinephrine in the sympathetic nerve-macrophage interplay. *J Neurochem* **75**, 2464–2471 (2000).

33. Elitsur, Y. *et al.* Neuropeptide Y (NPY) enhances proliferation of human colonic lamina propria lymphocytes. *Neuropeptides* **26**, 289–295 (1994).
34. Hernanz, A., Tato, E., De la Fuente, M., de Miguel, E. & Arnalich, F. Differential effects of gastrin-releasing peptide, neuropeptide Y, somatostatin and vasoactive intestinal peptide on interleukin-1 beta, interleukin-6 and tumor necrosis factor-alpha production by whole blood cells from healthy young and old subjects. *J. Neuroimmunol.* **71**, 25–30 (1996).
35. Nandakumar, S., Miller, C. W. & Kumaraguru, U. T regulatory cells: an overview and intervention techniques to modulate allergy outcome. *Clin Mol Allergy* **7**, 5 (2009).
36. Cross, L. J. *et al.* Neuropeptide Y-induced mast cell activation. *Biochem Soc Trans* **22**, 7S (1994).
37. Baxter, L. L., Watkins-Chow, D. E., Pavan, W. J. & Loftus, S. K. A curated gene list for expanding the horizons of pigmentation biology. *Pigment Cell Melanoma Res* **32**, 348–358 (2019).
38. Joost, S. *et al.* The Molecular Anatomy of Mouse Skin during Hair Growth and Rest. *Cell Stem Cell* **26**, 441-457.e7 (2020).
39. Pesce, J. T. *et al.* Retnla (Relmα/Fizz1) Suppresses Helminth-Induced Th2-Type Immunity. *PLoS Pathog* **5**, e1000393 (2009).
40. Nair, M. G., Cochrane, D. W. & Allen, J. E. Macrophages in chronic type 2 inflammation have a novel phenotype characterized by the abundant expression of Ym1 and Fizz1 that can be partly replicated in vitro. *Immunol Lett* **85**, 173–180 (2003).
41. Liu, T. *et al.* FIZZ1 stimulation of myofibroblast differentiation. *Am J Pathol* **164**, 1315–1326 (2004).
42. Keyes, B. E. *et al.* Impaired Epidermal to Dendritic T Cell Signaling Slows Wound Repair in Aged Skin. *Cell* **167**, 1323-1338.e14 (2016).
43. Ihunnah, C. A. *et al.* Estrogen sulfotransferase/SULT1E1 promotes human adipogenesis. *Mol Cell Biol* **34**, 1682–1694 (2014).
44. Kinlaw, W. B., Church, J. L., Harmon, J. & Mariash, C. N. Direct evidence for a role of the 'spot 14' protein in the regulation of lipid synthesis. *J Biol Chem* **270**, 16615–16618 (1995).
45. Strable, M. S. & Ntambi, J. M. Genetic control of de novo lipogenesis: role in diet-induced obesity. *Crit Rev Biochem Mol Biol* **45**, 199–214 (2010).
46. Miki, Y. *et al.* Lymphoid tissue phospholipase A2 group IID resolves contact hypersensitivity by driving antiinflammatory lipid mediators. *J Exp Med* **210**, 1217–1234 (2013).
47. Slominski, A. & Wortsman, J. Neuroendocrinology of the skin. *Endocr. Rev.* **21**, 457–487 (2000).
48. Laddha, N. C. *et al.* Association of Neuropeptide Y (NPY), Interleukin-1B (IL1B) Genetic Variants and Correlation of IL1B Transcript Levels with Vitiligo Susceptibility. *PLoS ONE* **9**, e107020 (2014).
49. Bakry, O., Mariee, A., Badr, I., Tayel, N. & El Gendy, S. NPY Gene Polymorphism in Vitiligo: A Case-Control Study in Egyptian Patients. *Indian J Dermatol* **65**, 65–67 (2020).
50. Suárez-Fariñas, M. *et al.* Nonlesional atopic dermatitis skin is characterized by broad terminal differentiation defects and variable immune abnormalities. *Journal of Allergy and Clinical Immunology* **127**, 954-964.e4 (2011).

51. Chen, E. Y. *et al.* Enrichr: interactive and collaborative HTML5 gene list enrichment analysis tool. *BMC Bioinformatics* **14**, 128 (2013).
52. Kuleshov, M. V. *et al.* Enrichr: a comprehensive gene set enrichment analysis web server 2016 update. *Nucleic Acids Res* **44**, W90-97 (2016).
53. Xie, Z. *et al.* Gene Set Knowledge Discovery with Enrichr. *Current Protocols* **1**, (2021).
54. Swindell, W. R. *et al.* Genome-Wide Expression Profiling of Five Mouse Models Identifies Similarities and Differences with Human Psoriasis. *PLoS ONE* **6**, e18266 (2011).
55. Quaranta, M. *et al.* Intraindividual genome expression analysis reveals a specific molecular signature of psoriasis and eczema. *Science Translational Medicine* **6**, 244ra90-244ra90 (2014).
56. Ahn, R. *et al.* RNA-seq and flow-cytometry of conventional, scalp, and palmoplantar psoriasis reveal shared and distinct molecular pathways. *Sci Rep* **8**, 11368 (2018).
57. Park, D., Jeong, H. O., Kim, B.-C., Ha, Y. M. & Young Chung, H. Computational approach to identify enzymes that are potential therapeutic candidates for psoriasis. *Enzyme Res* **2011**, 826784 (2011).
58. Roesner, L. M., Werfel, T. & Heratizadeh, A. The adaptive immune system in atopic dermatitis and implications on therapy. *Expert Rev Clin Immunol* **12**, 787–796 (2016).
59. Moosbrugger-Martinz, V., Tripp, C. H., Clausen, B. E., Schmuth, M. & Dubrac, S. Atopic dermatitis induces the expansion of thymus-derived regulatory T cells exhibiting a Th2-like phenotype in mice. *J Cell Mol Med* **20**, 930–938 (2016).
60. Lowes, M. A., Suárez-Fariñas, M. & Krueger, J. G. Immunology of psoriasis. *Annu Rev Immunol* **32**, 227–255 (2014).
61. Desai, S. R., Alexis, A. F. & Jacobson, A. Successful Management of a Black Male With Psoriasis and Dyspigmentation Treated With Halobetasol Propionate 0.01%/Tazarotene 0.045% Lotion: Case Report. *J Drugs Dermatol* **19**, 1000–1004 (2020).
62. Prinz, J. The Woronoff Ring in Psoriasis and the Mechanisms of Postinflammatory Hypopigmentation. *Acta Derm Venerol* **100**, 66–69 (2020).
63. Larrègue, M. *et al.* [Vitiligoid achromias and severe atopic dermatitis. Apropos of 4 cases]. *Ann Dermatol Venereol* **112**, 589–600 (1985).
64. Vachiramon, V. & Thadanipon, K. Postinflammatory hypopigmentation: Postinflammatory hypopigmentation. *Clinical and Experimental Dermatology* **36**, 708–714 (2011).

Figures

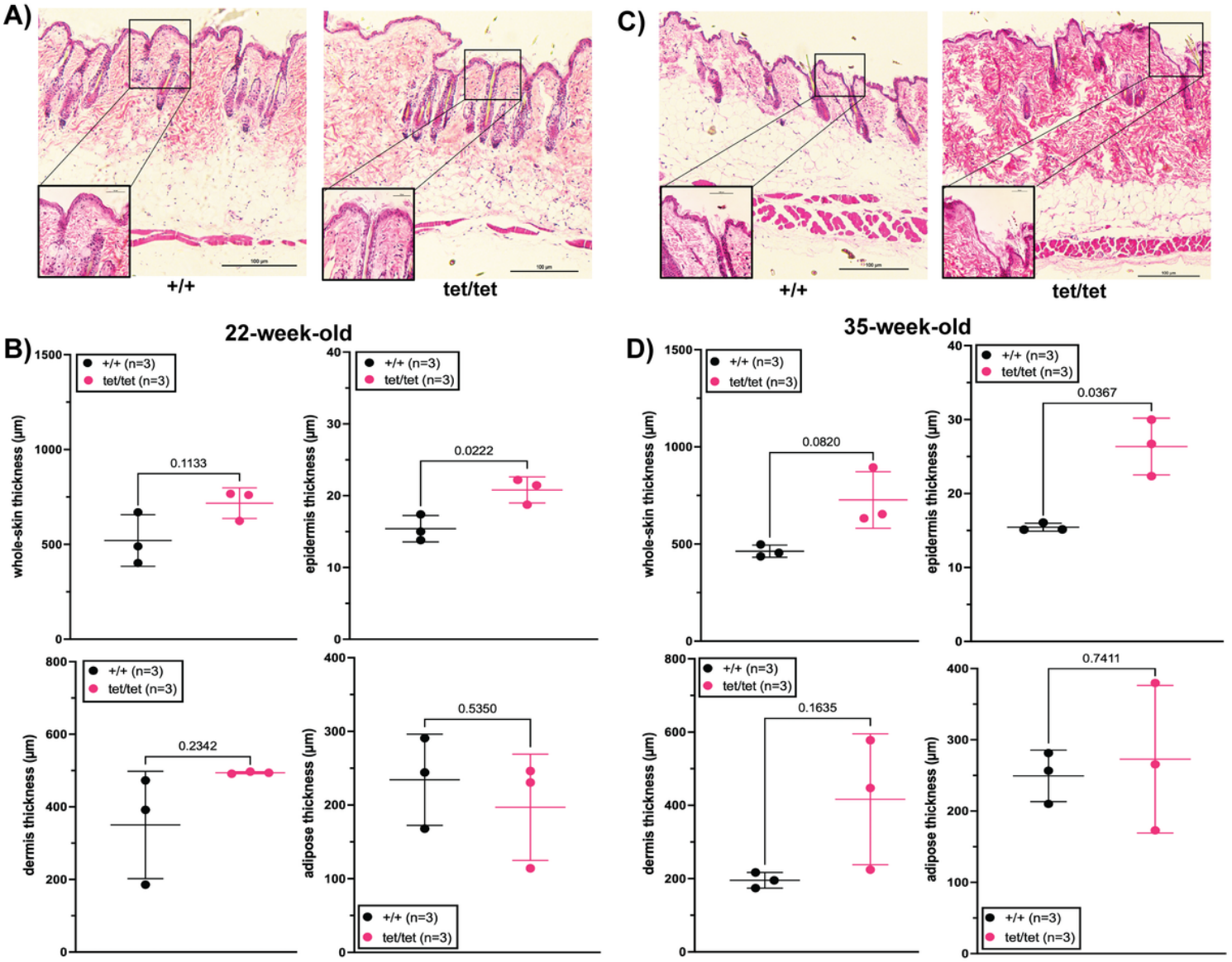

Figure 1

Fibrosis and epidermal thickening are observed in Npytet/tet skin. (A, C) Representative images of hematoxylin and eosin (H&E) staining of skin from Npy+/+ (n=3) and Npytet/tet (n=3) at 22 and 35 weeks old shows fibrosis in Npytet/tet skin. Scale bars: 100µm. (B, D) The average thickness of the whole skin, dermis, and subcutaneous adipose tissue are similar in both genotypes at 22 (B) and 35 (D) weeks old. The epidermis is thickened in the skin of Npytet/tet mice at both timepoints. Statistical significance was determined by unpaired t-test, p-values between comparisons are indicated on each graph, and p-values < 0.05 are considered statistically signficant.

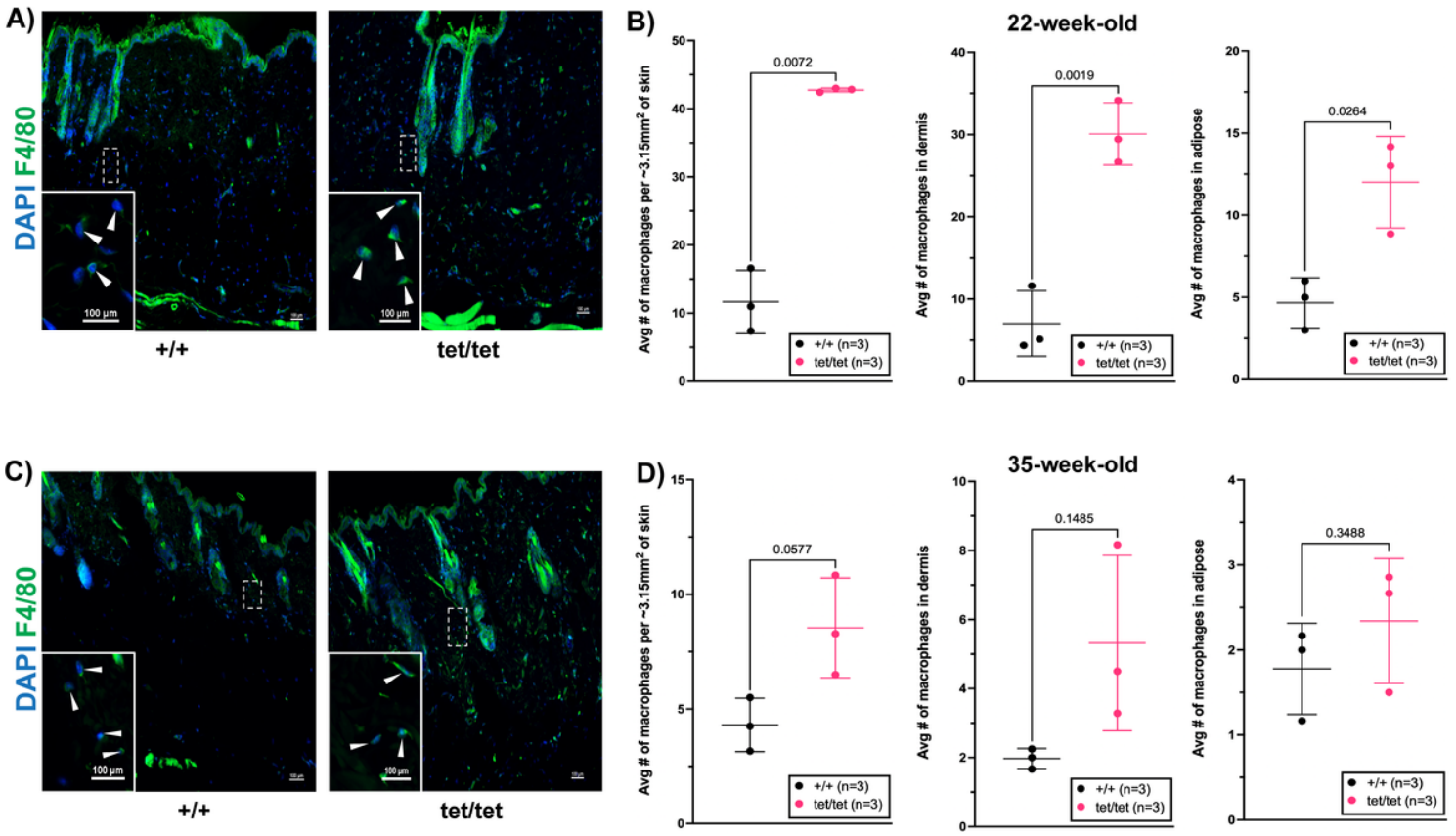

Figure 2

Macrophages infiltrate the skin of Npytet/tet mice. (A, C) Representative images of immunolabeled F4/80+ macrophages (green) in the skin of 22- and 35-week-old Npy+/+ (n=3) and Npytet/tet (n=3) mice. DAPI stains cell nuclei (blue). Scale bar: 100µm. (B) The average number of macrophages is significantly greater in 3.15mm2 of skin in 22-week-old Npytet/tet mice, which is attributed to their increased abundance in the dermis and subcutaneous adipose tissue. (D) The average number of macrophages shows a trend to be greater in 3.15mm2 of skin in 35-week-old Npytet/tet mice. Statistical significance was determined by unpaired t-test, p-values between comparisons are indicated on each graph, and p-values < 0.05 are considered statistically signficant.

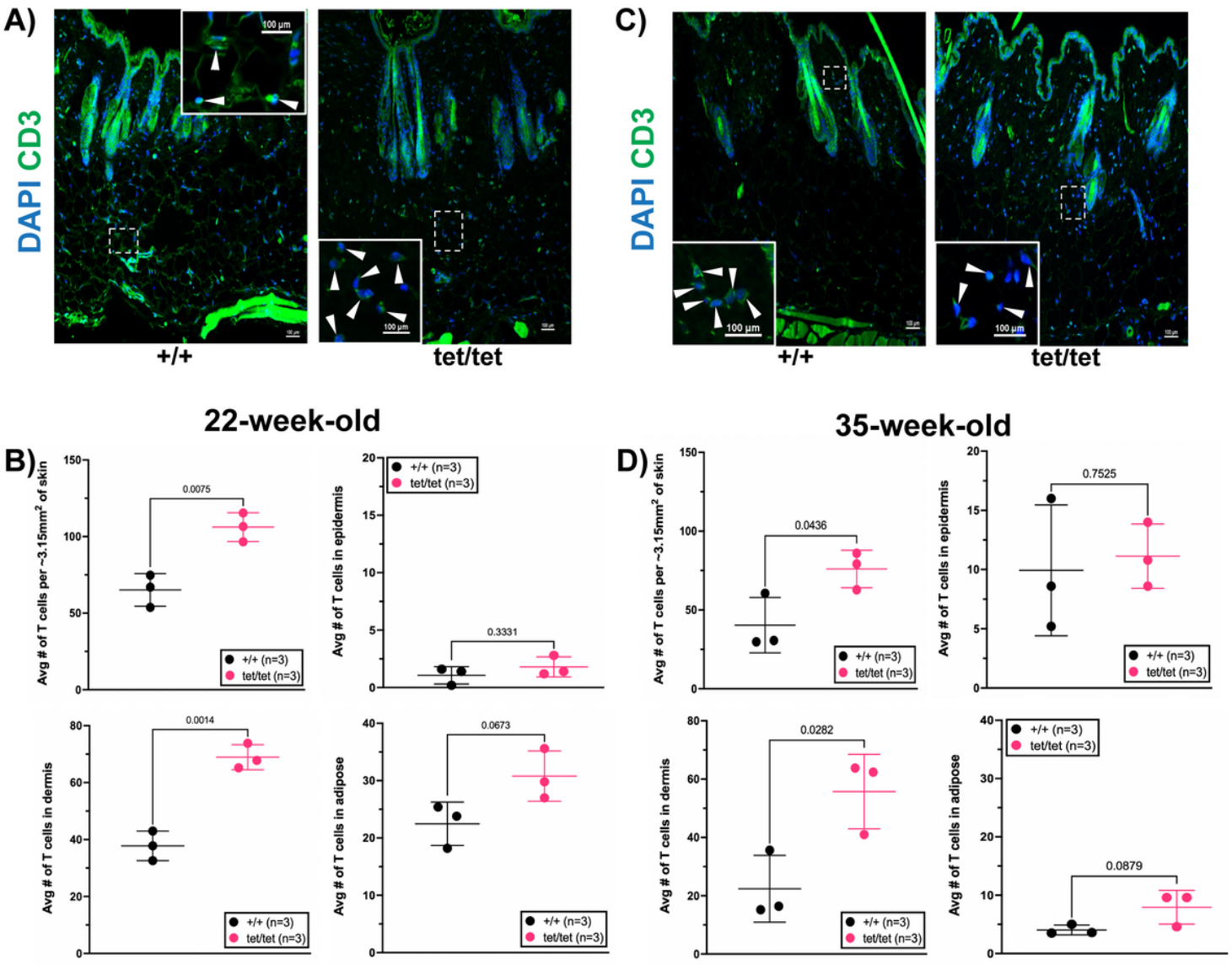

Figure 3

T cells are more abundant in Npytet/tet skin. (A, C) Representative images of immunolabeled CD3+ T cells (green) in the skin of 22- and 35-week-old Npy+/+ (n=3) and Npytet/tet (n=3) mice. DAPI stains cell nuclei (blue). Scale bar: 100µm. (B, D) The average number of T cells is significantly greater in 3.15mm2 of skin in 22- and 35-week-old Npytet/tet mice, which is attributed to their increased abundance in the dermis. Statistical significance was determined by unpaired t-test, p-values between comparisons are indicated on each graph, and p-values < 0.05 are considered statistically signficant.

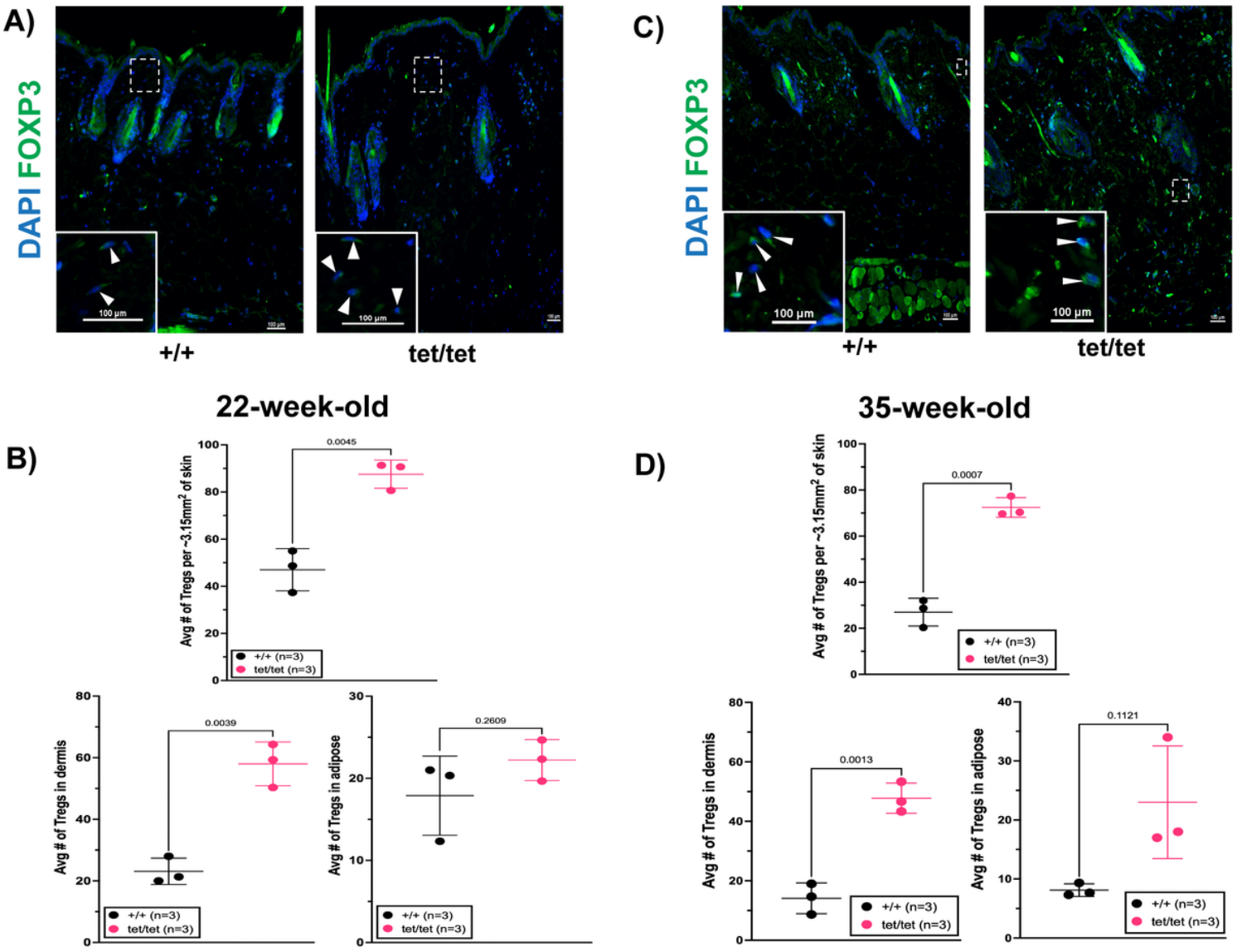

Figure 4

Tregs are more abundant in Npytet/tet skin. (A,C) Representative images of immunolabeled FOXP3+ Tregs (green) in the skin of 22- and 35-week-old Npy+/+ (n=3) and Npytet/tet (n=3) mice. DAPI stains cell nuclei (blue). Scale bar: 100µm. (B) The average number of Tregs is significantly greater in 3.15mm2 of skin in 22-week-old Npytet/tet mice, which is attributed to their increased abundance in the dermis. (D) The average number of Tregs is significantly greater in 3.15mm2 of skin in 35-week-old Npytet/tet mice, which is attributed to their increased abundance in the dermis and a trend for their increased abundance in the subcutaneous adipose tissue. Statistical significance was determined by unpaired t-test, p-values between comparisons are indicated on each graph, and p-values < 0.05 are considered statistically signficant.

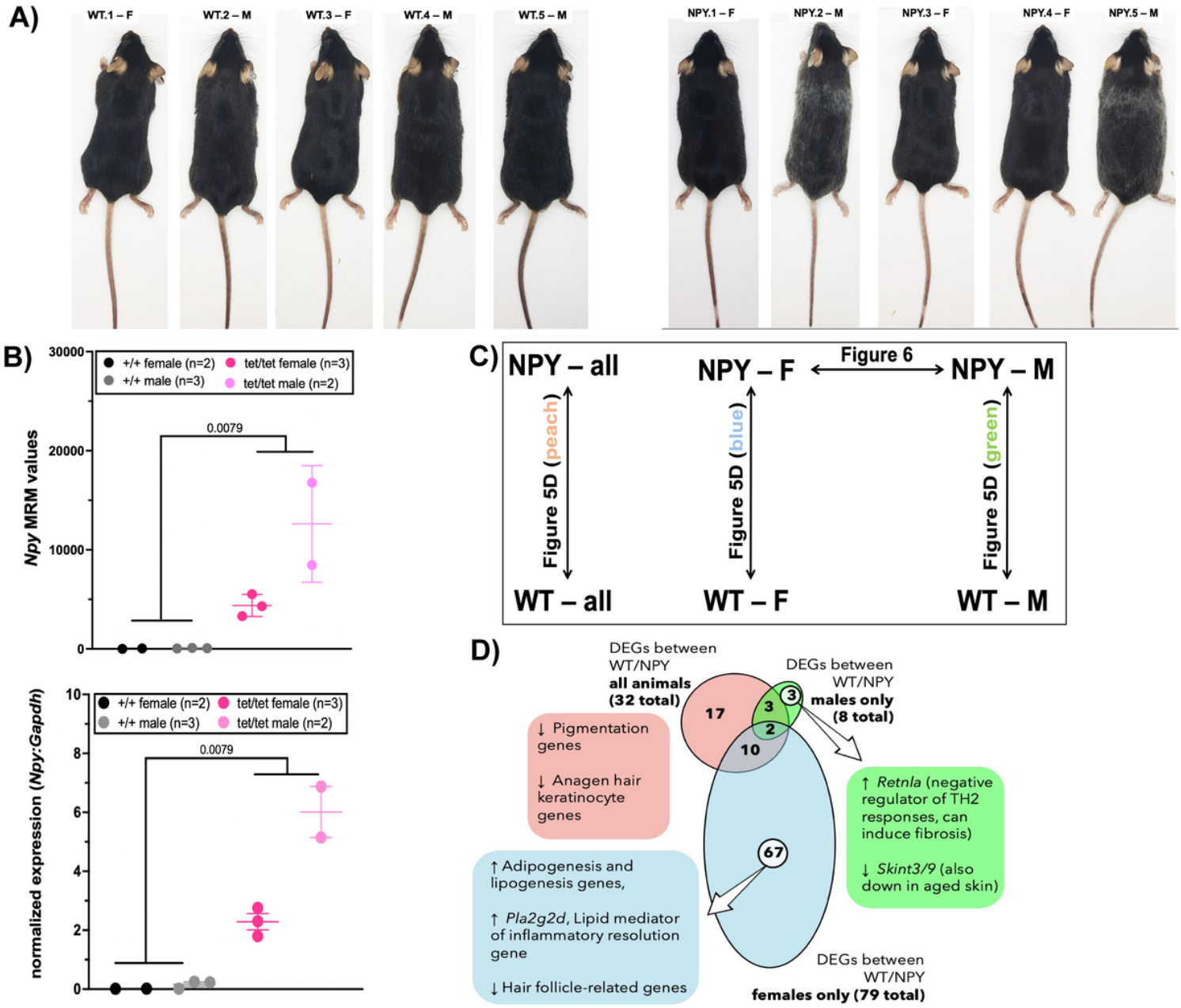

Figure 5

Transcriptomic changes in skin reinforce the pathologic presentation in Npytet/tet mice. (A) Representative images of 22-week-old Npy+/+ (n=5) and Npytet/tet (n=5) mice whose skin was analyzed via RNAseq. In this cohort of mice, two Npytet/tet mice exhibited advanced hair graying, and both were males. WT = Npy+/+; NPY = Npytet/tet; F = female; M = male. (B) Quantification of Npy transcripts in Npy+/+ and Npytet/tet skin via RNAseq (MRM values) and qPCR (normalized expression) shows that Npy is significantly elevated in Npytet/tet skin. (C) A schematic of the comparison strategies employed to evaluate the RNAseq data. (D) A Venn diagram representing the number of DEGs in Npy+/+ versus Npytet/tet comparing all animals (32 DEGs), in female Npy+/+ versus female Npytet/tet comparison (79 DEGs), and in male Npy+/+ versus male Npytet/tet comparison (8 DEGs).

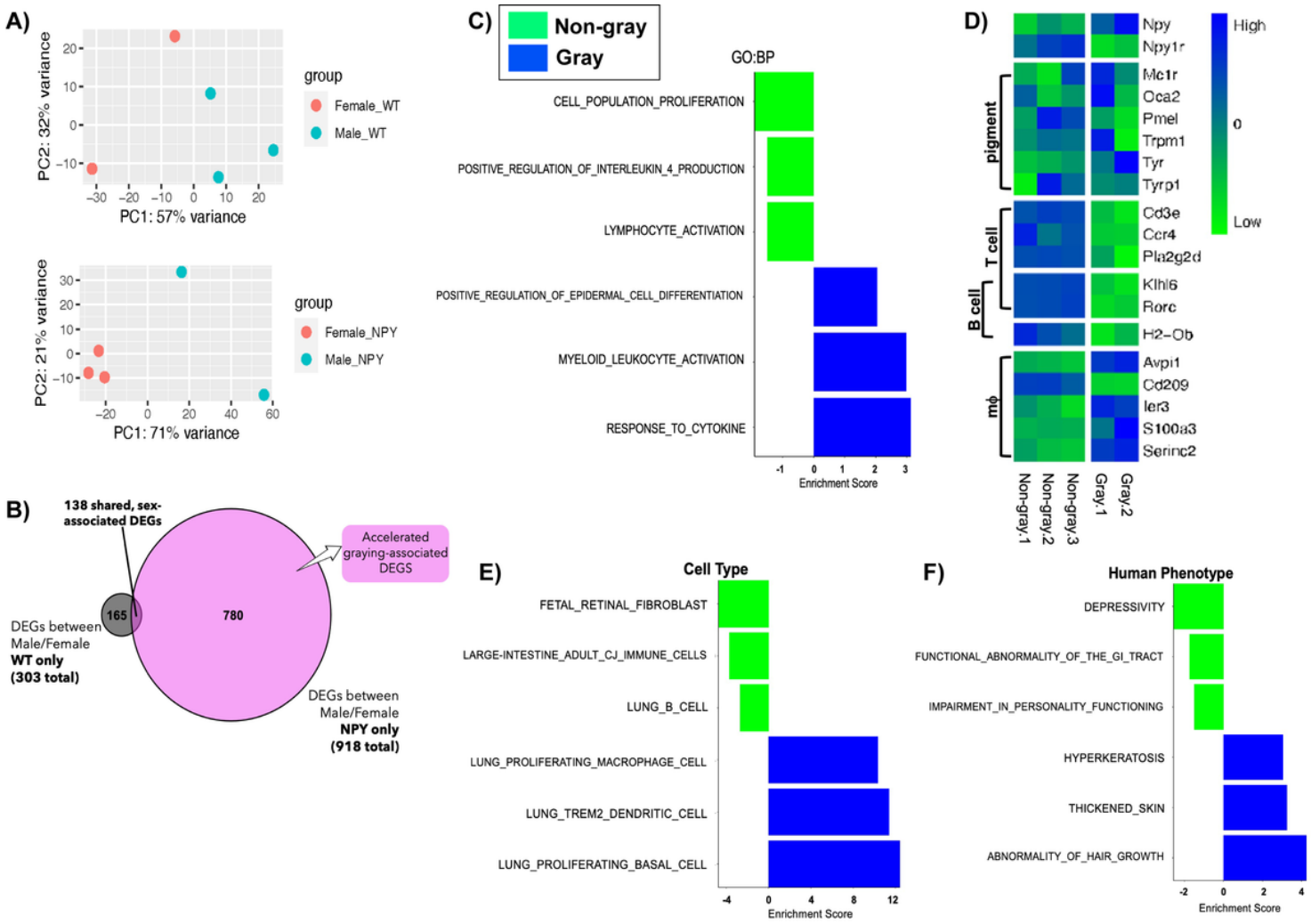

Figure 6

Non-gray Npytet/tet skin is enriched for inflammation, and gray Npytet/tet skin is enriched for skin pathology. A) PCA plots comparing samples within Npy+/+ or Npytet/tet groups show that graying and/or sex influences the variations within genotypes. (B) A Venn diagram representing the number of DEGs when comparing between sexes of Npy+/+ (303 DEGs) or Npytet/tet (918 DEGs) groups. The 138 DEGs that were common, sex-associated genes were removed from downstream analyses. (C) Clustered bar graph depicting the Gene Ontology: Biological Processes that are upregulated in non-gray Npytet/tet skin (green) compared to gray Npytet/tet skin (blue). The legend (box) indicates that for panels C, E, and F, non-gray Npytet/tet samples are shown in green, and gray Npytet/tet samples are shown in blue. (D) A heatmap of some of the top DEGs in non-gray vs gray Npytet/tet skin shows an enrichment for T and B cells in non-gray skin in contrast to an enrichment for macrophages in gray skin. (E) Clustered bar graph depicting the Cell Types that are enriched in non-gray Npytet/tet skin (green) compared to gray Npytet/tet skin (blue). (F) Clustered bar graph depicting the Human Phenotype Ontologies that are enriched in non-gray Npytet/tet skin (green) compared to gray Npytet/tet skin (blue).

Supplementary Files

This is a list of supplementary files associated with this preprint. Click to download.

- NPYRNAseqSupplementaryFile.xlsx
- SupplementaryFigures.docx